



COVER PAGE

Document downloaded by @DAEL

Wed Apr 22 20:31:45 2026

For personal use

When automatic English translation is provided, only the original document is authentic.

The EAA cannot be held responsible of any translation error

Bibliographical reference

Intensity Potential Approach for Modeling High-Frequency Sound Fields,
Michael Thivant, Patrik B. U. Andersson and Jean-Louis Guyader, *Acta Acustica* **vol. 97** (Number 1), 2011, pp. 103-114

DOI

<https://doi.org/10.3813/AAA.918391>

Intensity Potential Approach for Modeling High-Frequency Sound Fields

Michael Thivant¹⁾, Patrik B. U. Andersson²⁾, Jean-Louis Guyader³⁾

¹⁾ Vibratec, 28, Chemin du Petit Bois, 69131 Ecully, France. michael.thivant@vibratec.fr

²⁾ Division of Applied Acoustics, Chalmers University of Technology, 412 96 Göteborg, Sweden.
patrik.andersson@chalmers.se

³⁾ Laboratoire Vibrations Acoustique, INSA de Lyon, 25 bis, Avenue Jean Capelle, 69621 Villeurbanne Cedex, France. jean-louis.guyader@insa-lyon.fr

Summary

This paper proposes the intensity potential approach for prediction of high-frequency sound power radiation. The approach is based on the Helmholtz decomposition of the vector field of time-averaged sound intensity into its irrotational and rotational components. The local power balance in a lossless medium is expressed in terms of the irrotational component only, and results in the Poisson equation for a scalar intensity potential of this component only. The approach gives an exact expression for the sound power through any closed surface in terms of the irrotational component, provided that the boundary conditions are correct. The approach is evaluated by exploring the two intensity components in three canonical examples, and by comparison to measured data with special focus on directivity aspects. It is concluded that the intensity potential approach is relevant, in particular for high-frequency sound fields from multiple sources that are uncorrelated and broadbanded. However, the intensity is generally overestimated in the shadow zones and underestimated in the directly exposed regions. Further, peaks in narrow frequency bands associated with interference of waves are ignored.

PACS no. 43.20.Rz, 43.55.Ka

1. Introduction

This paper presents and demonstrates the intensity potential approach. The method is based on the local power balance in a lossless medium and the Helmholtz decomposition of the active intensity vector into its irrotational and rotational components. Sound power flow can be predicted by limiting the problem to the irrotational intensity and the determination of its potential. The resulting equation is a Poisson equation analogous to acoustic diffusion or heat transfer. The approach is suitable for prediction of sound power flow from sources in partial enclosures to the far field. This kind of problem is frequently encountered in transport and machinery noise prediction, where the encapsulations of engines and auxiliary devices form partial enclosures.

Efficient and robust methods for prediction of radiated sound in the mid and high-frequency range are of general interest. The methods should be efficient in terms of low computational cost (short computation time and low memory requirement) and in terms of simplicity in determining representative boundary conditions.

The measured response at one specific frequency can vary strongly between nominally identical objects (e.g. be-

tween objects from the same production line). The methods should therefore be robust in terms of being relatively insensitive to geometrical details and boundary conditions so that the general behavior of objects of similar design can be predicted, rather than the exact response of a single individual object.

Classical methods based on the Helmholtz equation or integral formulation are quite accurate in the low frequency range for simple geometry. Examples of such approaches are the finite element method for the Helmholtz equation and boundary element methods for the Kirchhoff-Helmholtz integral equation. However, they are limited for industrial problems since they are time-consuming and lack robustness in the mid and high frequency range.

Therefore, methods based on spatial and frequency averages of energetic and kinetic variables have been developed. Most notable are statistical energy analysis, ray-tracing techniques, frequency-averaged boundary element formulations, and acoustic diffusion approaches. The methods aim to describe sound fields with energy paths. The main advantages of these methods are much lower computing time, smoother solutions, and above all better robustness. The development and basic principles of statistical energy analysis are concisely outlined in the paper by Burroughs *et al.* [1], while more detailed information is found in the book by Lyon and DeJong [2]. A concise presentation of the ray-tracing technique is for

Received 5 July 2010,
accepted 2 November 2010.

instance found in [3], where also a formal proof is proposed that shows that the ray-tracing technique with a diffuse reflection law is equivalent to an integral formulation of power balance. Several boundary integral formulations have been proposed lately. Guyader and Loyau [4] derived an integral equation for the frequency-averaged quadratic pressure starting from the explicit Rayleigh integral. The method is applicable for free-field radiation from planar structures. In line with this concept, Kim and Ih [5] derived a boundary element method for predicting sound pressure level at high frequencies bands. They simplify the calculations by neglecting the cross-spectra of sound pressure or acceleration between two positions on the radiating surface by assuming that it is much smaller than the auto-spectra. Guyader [6] generalised the integral equation for the frequency-average quadratic pressure by using only a single assumption, the statistical independence of boundary pressure and velocity and of the Green's function. Franzoni *et al.* [7] have proposed a boundary element method formulated in terms of time-averaged energy and intensity variables by using a broadband acoustic energy/intensity source. Kuttruff [8] and Lindqvist [9] assumed random diffusion processes to develop mathematical models describing the expected density of sound particles in rooms. More recent, Picaut and co-workers [10, 11, 12] extended the application of the diffusion model to a variety of enclosure types. Schmitt [13, 14] added the direct field of sources to the acoustic diffusion model and he included diffraction in the integral formulation based on the local energy balance at surfaces.

Classical diffusion equations, dedicated to either structural vibrations or acoustics, deal with the total acoustic energy, which is the sum of the potential and the kinetic energies. For a stationary problem and a sufficient integration time, the time-averaged total acoustic energy is independent of time and is denoted $E(\mathbf{r})$. Constitutive equations are the local power balance:

$$\nabla \cdot \mathbf{I}(\mathbf{r}) = -\eta\omega E(\mathbf{r}), \quad (1)$$

written here at a point \mathbf{r} without any sources (sources can be taken into account in boundary conditions), and an assumption on the sound field

$$\mathbf{I}(\mathbf{r}) = -D\nabla E(\mathbf{r}), \quad (2)$$

where $\mathbf{I}(\mathbf{r})$ is the active sound intensity that is a time-averaged quantity independent of time (see details in section 2), η the damping loss factor, and ω the angular frequency. equation (1) is valid for any type of wave, but equation (2) has only been demonstrated for certain types of waves. For damped free waves, D is related to group velocity [15, 16, 17], and for diffuse fields it can be linked with the mean free path between obstacles [11]. equation (2) is analogous to Fourier's law encountered in heat transfer problems. It states that energy flows from zones of high energy density to zones of lower density. Combining equations (1) and (2) leads to the classical diffusion equation

$$\Delta E(\mathbf{r}) - \frac{\eta\omega}{D} E(\mathbf{r}) = 0. \quad (3)$$

The intensity potential approach results in an acoustic diffusion type of equation, but it differs from the classical one in two respects. First, the introduction of the *intensity potential* instead of an acoustic energy variable results in an equation that does not violate the geometrical divergence of acoustic energy in free field. The energy variable in the classical acoustic diffusion equation does not capture the correct geometrical divergence in free field [16]. Second, the relation between the intensity potential and the intensity is given directly by the Helmholtz decomposition; no additional assumption of a relation of the Fourier law type is needed. Further, the diffusion equation obtained by the intensity potential approach is directly computable by using common heat transfer finite element software.

The intensity potential approach is based on the decomposition of the active intensity into its irrotational and rotational components according to the Helmholtz theorem. The structure and patterns of acoustic intensity fields in terms of the active and reactive intensities, their rotational and irrotational components, and the kinetic, potential and Lagrangian energies have been extensively studied by Pascal [18, 19] and Pascal and Li [20].

This paper is organized as follows. Section 2 gives the theoretical formulation. It presents the local power balance for a stationary sound field and the Helmholtz decomposition of the vector field of active intensity. The rotational and irrotational components are further elaborated and the resulting Poisson equation for the intensity potential is derived. The boundary conditions needed to model sources and acoustically rigid objects are presented. Section 3 illustrates the properties of active intensity and its components of the Helmholtz decomposition through three examples of simple intensity fields. Section 4 evaluates the method by comparison to measured data. Finally, the work is concluded.

2. Theoretical formulation

Figure 1 shows the nomenclature used to describe sound power flow from acoustic sources in an infinite acoustic domain Ω . Bodies with the boundary surface Γ might be present in the domain. The instantaneous sound intensity in a position $\mathbf{r} \in \Omega$ and time t is defined as

$$\mathbf{I}(\mathbf{r}, t) = p(\mathbf{r}, t) \mathbf{u}(\mathbf{r}, t), \quad (4)$$

where $p(\mathbf{r}, t)$ is the sound pressure and $\mathbf{u}(\mathbf{r}, t)$ the particle velocity vector. The time average of the instantaneous sound intensity is expressed as

$$\bar{\mathbf{I}}(\mathbf{r}, \tau) = \frac{1}{T} \int_{\tau}^{\tau+T} \mathbf{I}(\mathbf{r}, t) dt, \quad (5)$$

where T is the integration time.

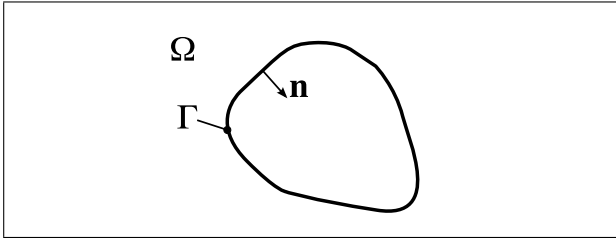


Figure 1. The infinite acoustic domain Ω may contain objects with boundary Γ . The surface normal \mathbf{n} is defined to point out of the domain into the objects.

For a stationary phenomenon and when the integration time is sufficient, the time-average intensity is constant with τ . This is assumed in the rest of the paper and, for brevity, it will be noted $\mathbf{I}(\mathbf{r})$ and is referred to as the active intensity. In each point of the domain, this active intensity vector describes the resulting direction and magnitude of the flow of acoustic power per unit area.

In many practical applications the volume dissipation is very small in comparison to the absorption at the boundaries. Thus, the volume dissipation is neglected and a simple relation gives the local energy balance for a stationary sound field according to

$$\nabla \cdot \mathbf{I}(\mathbf{r}) = \Pi_{\text{in}}(\mathbf{r}), \quad (6)$$

where $\nabla \cdot \mathbf{I}(\mathbf{r})$ is the divergence of the active intensity and $\Pi_{\text{in}}(\mathbf{r})$ is the volume density of sound power sources as a function of position \mathbf{r} .

2.1. Helmholtz theorem

According to the Helmholtz decomposition, any continuous vector field whose divergence and curl vanish at infinity can be decomposed as the sum of an irrotational (curl-free/laminar) part and a rotational (divergence-free/solenoidal) part (see [21, pp. 95–101]). This property applies to the active intensity in absence of sound sources at infinity. Thus, the intensity vector may be decomposed as the sum of the gradient of a scalar potential and the curl of a vector potential [19],

$$\mathbf{I}(\mathbf{r}) = \mathbf{I}_{\phi}(\mathbf{r}) + \mathbf{I}_{\mathbf{C}}(\mathbf{r}), \quad (7)$$

where

$$\mathbf{I}_{\phi}(\mathbf{r}) = -\nabla\phi(\mathbf{r}) \quad \text{and} \quad \mathbf{I}_{\mathbf{C}}(\mathbf{r}) = \nabla \times \mathbf{C}(\mathbf{r}). \quad (8)$$

This decomposition is unique but the scalar potential $\phi(\mathbf{r})$ and the vector potential $\mathbf{C}(\mathbf{r})$ are defined including a constant and a gradient, respectively. Indeed, the gradient of a constant and the curl of a gradient are zero, i.e. the two components of the intensity are unchanged by the following transforms:

$$-\nabla(\phi(\mathbf{r}) + \phi_0) = -\nabla\phi(\mathbf{r}), \quad (9)$$

$$-\nabla \times (\mathbf{C}(\mathbf{r}) + \nabla\chi(\mathbf{r})) = -\nabla \times \mathbf{C}(\mathbf{r}), \quad (10)$$

where $\chi(\mathbf{r})$ is any continuously differentiable scalar function. It is customary to choose the constant ϕ_0 so that the scalar potential tends towards zero at infinity and the gradient $\nabla\chi(\mathbf{r})$ so that the divergence of the vector potential is zero. Then, in an unbounded volume Ω , the scalar potential $\phi(\mathbf{r})$ and the vector potential $\mathbf{C}(\mathbf{r})$ are obtained by integrating the divergence and the curl of $\mathbf{I}(\mathbf{r})$ over Ω , respectively (see [21, pp. 95–101]):

$$\phi(\mathbf{r}) = \frac{1}{4\pi} \iiint_{\Omega} \frac{\nabla \cdot \mathbf{I}(\mathbf{r}')}{R} d\Omega(\mathbf{r}') \quad (11)$$

and

$$\mathbf{C}(\mathbf{r}) = \frac{1}{4\pi} \iiint_{\Omega} \frac{\nabla \times \mathbf{I}(\mathbf{r}')}{R} d\Omega(\mathbf{r}'), \quad (12)$$

where $R = \|\mathbf{r}' - \mathbf{r}\|$ is the distance between the points \mathbf{r} and \mathbf{r}' .

In a volume $\Omega' \subseteq \Omega$ limited by a closed surface Γ' these relations become

$$\begin{aligned} \phi(\mathbf{r}) = & \iiint_{\Omega'} \frac{\nabla \cdot \mathbf{I}(\mathbf{r}')}{4\pi R} d\Omega(\mathbf{r}') \\ & - \iint_{\Gamma'} \frac{\mathbf{I}(\mathbf{r}') \cdot \mathbf{n}(\mathbf{r}')}{4\pi R} d\Gamma(\mathbf{r}') \end{aligned} \quad (13)$$

and

$$\begin{aligned} \mathbf{C}(\mathbf{r}) = & \iiint_{\Omega'} \frac{\nabla \times \mathbf{I}(\mathbf{r}')}{4\pi R} d\Omega(\mathbf{r}') \\ & + \iint_{\Gamma'} \frac{\mathbf{I}(\mathbf{r}') \times \mathbf{n}(\mathbf{r}')}{4\pi R} d\Gamma(\mathbf{r}'). \end{aligned} \quad (14)$$

Equation (13) shows that the scalar potential of intensity $\phi(\mathbf{r})$ is expressed directly as a function of the injected or absorbed power. It depends on the volume density $\nabla \cdot \mathbf{I}(\mathbf{r})$ of sources (or sinks) of sound power distributed in the domain according to equation (6), and the surface density $\mathbf{I}(\mathbf{r}) \cdot \mathbf{n}(\mathbf{r})$ of sources (or sinks) distributed on the boundary. On the contrary, the vector potential $\mathbf{C}(\mathbf{r})$ in equation (14) is expressed in terms of sources that do not dissipate or inject acoustic energy, but only perturb the intensity field.

Some general properties of the rotational and irrotational components are presented in the following sections, while section 3 further illustrates the behavior of the active intensity and its irrotational and rotational components for some canonical examples.

2.2. Rotational intensity

Equation (14) shows that the vector potential $\mathbf{C}(\mathbf{r})$ depends on the tangential components of the intensity vector $\mathbf{I}(\mathbf{r}) \times \mathbf{n}(\mathbf{r})$ on the boundary surfaces. These components are directed in the plane of the surface and do not dissipate or inject acoustic energy. The vector potential $\mathbf{C}(\mathbf{r})$ also depends on the volume sources $\nabla \times \mathbf{I}(\mathbf{r})$. These sources are not power sources, but sources perturbing the intensity field to create, for example, vortices of acoustic energy in

the fluid. The local energy balance associated with the rotational intensity is characterized by a right-hand side that is zero at every point in the fluid. Indeed, the divergence of a rotation is always zero:

$$\nabla \cdot \mathbf{I}_C(\mathbf{r}) = \nabla \cdot (\nabla \times \mathbf{C}(\mathbf{r})) = 0. \quad (15)$$

By using the divergence theorem, the global energy balance related to the rotational intensity may be written in the form of a surface or volume integral according to

$$\begin{aligned} \iint_{\Gamma'} \mathbf{I}_C(\mathbf{r}') d\Gamma(\mathbf{r}') &= \iint_{\Gamma'} (\nabla \times \mathbf{C}(\mathbf{r}')) d\Gamma(\mathbf{r}') \\ &= \iiint_{\Omega'} \nabla \cdot (\nabla \times \mathbf{C}(\mathbf{r}')) d\Omega(\mathbf{r}') \\ &= 0. \end{aligned} \quad (16)$$

Thus, also the global balance is zero for any volume Ω' bounded by a closed surface Γ' .

Another fundamental property of a rotational field concerns its streamlines. By definition, they are tangents to the vector $\mathbf{I}_C(\mathbf{r})$ at every point \mathbf{r} . Thus, they describe the path taken by the energy carried by $\mathbf{I}_C(\mathbf{r})$. However, because of its rotational nature, the streamlines of $\mathbf{I}_C(\mathbf{r})$ cannot start or end on a source or sink of energy; they can only form closed loops or start and end at infinity. Section 3 shows examples illustrating this property.

2.3. Irrotational intensity and Poisson's equation for intensity potential

By using the Helmholtz decomposition, the divergence of the acoustic intensity is rewritten according to

$$\begin{aligned} \nabla \cdot \mathbf{I}(\mathbf{r}) &= \nabla \cdot \mathbf{I}_\phi(\mathbf{r}) + \nabla \cdot \mathbf{I}_C(\mathbf{r}) \\ &= \nabla \cdot \nabla \phi(\mathbf{r}) + \nabla \cdot (\nabla \times \mathbf{C}(\mathbf{r})) \\ &= -\Delta \phi(\mathbf{r}) + 0. \end{aligned} \quad (17)$$

Thus, the local acoustic energy balance (6) can be rewritten as

$$-\Delta \phi(\mathbf{r}) = \Pi_{inj}(\mathbf{r}). \quad (18)$$

This is the Poisson equation. It is formally identical to the equation that governs the temperature distribution for stationary problems of heat conduction in isotropic media.

For a right-hand side of sources and sinks of power w_i localized at the points \mathbf{r}_i , the relation (18) is written as

$$-\Delta \phi(\mathbf{r}) = \sum_i w_i \delta(\mathbf{r}, \mathbf{r}_i). \quad (19)$$

This equation highlights the fact that the scalar field $\phi(\mathbf{r})$, and thus the irrotational intensity $\mathbf{I}_\phi(\mathbf{r})$, are directly connected to the sources and sinks of power w_i .

The sound power flowing through a closed surface Γ' is rewritten by using (17) according to

$$\begin{aligned} \iint_{\Gamma'} \mathbf{I}(\mathbf{r}') \cdot \mathbf{n}(\mathbf{r}') d\Gamma(\mathbf{r}') &= \iiint_{\Omega'} \nabla \cdot \mathbf{I}(\mathbf{r}') d\Omega(\mathbf{r}') \\ &= \iiint_{\Omega'} \nabla \cdot \mathbf{I}_\phi(\mathbf{r}') d\Omega(\mathbf{r}') \\ &= \iint_{\Gamma'} \mathbf{I}_\phi(\mathbf{r}') \cdot \mathbf{n}(\mathbf{r}') d\Gamma(\mathbf{r}'). \end{aligned} \quad (20)$$

Hence, the injected or absorbed power at the boundary surfaces is expressed only as a function of the irrotational intensity. It is reasonable to describe the propagation of acoustic energy by using only the irrotational component of intensity.

2.4. Boundary conditions

The solution of the Poisson equation (18) requires not only the distribution of the volume sources of power $\Pi_{in}(\mathbf{r})$, but also the boundary conditions on the boundaries Γ of the considered domain Ω . They can be expressed in terms of the intensity potential $\phi(\mathbf{r})$ or in terms of the normal component of the irrotational intensity,

$$I_{\phi_n}(\mathbf{r}) = \mathbf{I}_\phi(\mathbf{r}) \cdot \mathbf{n}(\mathbf{r}) = -\frac{\partial \phi(\mathbf{r})}{\partial \mathbf{n}(\mathbf{r})}, \quad (21)$$

where $\mathbf{n}(\mathbf{r})$ is the unit normal vector at \mathbf{r} , and $\partial/\partial \mathbf{n}(\mathbf{r}) = \mathbf{n}(\mathbf{r}) \cdot \nabla$ represents the directional derivative in the direction $\mathbf{n}(\mathbf{r})$. If the distribution of $\phi(\mathbf{r})$ or $I_{\phi_n}(\mathbf{r})$ is known on the boundary surfaces, one can write the Dirichlet or Neuman conditions according to

$$\phi(\mathbf{r}) = \phi_0(\mathbf{r}) \quad \text{for } \mathbf{r} \in \Gamma_{\phi_0} \quad (22)$$

and

$$\frac{\partial \phi(\mathbf{r})}{\partial \mathbf{n}(\mathbf{r})} = -I_{\phi_{n0}}(\mathbf{r}) \quad \text{for } \mathbf{r} \in \Gamma_{I_{\phi_{n0}}}, \quad (23)$$

where $\Gamma_{\phi_0} \subseteq \Gamma$ and $\Gamma_{I_{\phi_{n0}}} \subseteq \Gamma$ are the portions of the boundary with each boundary condition.

In addition, equation (13) suggests that the boundary conditions can alternatively be expressed as a function of the normal component of the active intensity, $\mathbf{I}(\mathbf{r}) \cdot \mathbf{n}(\mathbf{r})$. Thus, we have the choice to express the boundary conditions in terms of either the total active intensity or only its irrotational component. The rotational component $\mathbf{I}_C(\mathbf{r})$ has no influence on the potential $\phi(\mathbf{r})$ or the irrotational component $\mathbf{I}_\phi(\mathbf{r})$.

2.4.1. Power sources

Under the intensity potential approach, the sound radiation from a vibrating object is ideally modeled by the surface distribution of the normal component of intensity $\mathbf{I}_{\phi_n}(\mathbf{r})$. The boundary condition is then of Neuman type (equation 23). When $I_{\phi_n}(\mathbf{r})$ is constant on a surface $\Gamma_{I_{\phi_n}}$ with area S_0 , the boundary condition on this surface is expressed in terms of the total radiated power w_{S_0} ,

$$\frac{\partial \phi(\mathbf{r})}{\partial \mathbf{n}(\mathbf{r})} = -I_{\phi_n}(\mathbf{r}) = -\frac{w_{S_0}}{S_0} \quad \text{for } \mathbf{r} \in \Gamma_{I_{\phi_n}}. \quad (24)$$

The power of the acoustic point sources may be taken into account in the right-hand side of the Poisson equation (18) and can be modeled by a heat point source in a heat transfer software.

2.4.2. Reflecting surfaces

A reflecting boundary such as a rigid wall does not allow power to flow over its boundary. Thus, it is described by a normal component of the intensity that is zero,

$$\frac{\partial \phi(\mathbf{r})}{\partial \mathbf{n}(\mathbf{r})} = 0 \quad \text{for } \mathbf{r} \in \Gamma_0, \quad (25)$$

where $\Gamma_0 \subseteq \Gamma$ is the portion of the boundary with reflecting boundary.

2.4.3. Radiation in free field

The Poisson equation including the boundary conditions can be solved by the Finite Element Method in a finite volume. For the radiation in an open space, the acoustic medium is unbounded and the direct use of Finite Element is impossible. To avoid that difficulty, we introduced a virtual surface whose boundary condition minimizes the difference from the unbounded domain solution. In practice, we used a spherical surface located far from the sound source and applied the radiation boundary condition (see Appendix for demonstration)

$$I_{\phi_R}(R, \theta, \phi) = -\frac{\partial \phi(R, \theta, \phi)}{\partial R} = \frac{1}{R} \phi(R, \theta, \phi), \quad (26)$$

where (R, θ, ϕ) are the coordinates in a spherical coordinate system of points located on the sphere far from the sound source, and $\partial/\partial R$ represents the derivative with respect to the radial distance R . This approach produces satisfactory calculation for points located around the sphere centre; the bigger the sphere radius, the larger the calculation zone. When the radius tends to infinity, the boundary condition is known as Sommerfeld's conditions and the calculation would be accurate for all points at finite distances from the object, but of course this is impossible when using the Finite Element Method.

The thermal analogy of this relationship is an exchange by convection with a constant coefficient equal to $1/R$. This relationship is used to find the minimum distance R as a function of the dimensions of the problem.

3. Examples of intensity fields

The following examples illustrate the properties of the active intensity and its decomposition by using the Helmholtz theorem.

3.1. Interference between a propagating wave and a standing wave

Pascal [18] studied the interference patterns created by plane waves. He explained the relations between the different energy variables: the active and reactive intensities, their irrotational and rotational components, and the kinetic, potential and Lagrangian energies.

To illustrate the behavior of the total active intensity and its irrotational and rotational components, an example of interference between two perpendicular plane waves

is repeated here for the case of a wave propagating in x -direction and a standing wave in y -direction. The complex amplitude of the pressure is equal to the sum of the contributions of the waves,

$$p(x, y) = Ae^{-jkx} + 2B \cos(ky), \quad (27)$$

and the corresponding active intensity is

$$\mathbf{I}(x, y) = \left[\frac{A^2}{2\rho c} + \frac{AB}{\rho c} \cos(kx) \cos(ky) \right] \mathbf{e}_x + \frac{AB}{\rho c} \sin(kx) \sin(ky) \mathbf{e}_y, \quad (28)$$

where \mathbf{e}_x and \mathbf{e}_y are unit vectors in the x - and y -directions, respectively. The irrotational active intensity comes only from the propagating plane wave,

$$\mathbf{I}_\phi(x, y) = \frac{A^2}{2\rho c} \mathbf{e}_x. \quad (29)$$

Thus, the scalar potential associated with it is identical to that of the propagating wave alone,

$$\phi(x, y) = -\frac{A^2}{2\rho c} x + \phi_0. \quad (30)$$

The rotational intensity is given by

$$\mathbf{I}_C(x, y) = \frac{AB}{2\rho c} \left[\cos(k(x-y))(\mathbf{e}_x + \mathbf{e}_y) + \cos(k(x+y))(\mathbf{e}_x - \mathbf{e}_y) \right], \quad (31)$$

and the vector potential by

$$\mathbf{C}(x, y) = \frac{AB}{2\rho c} \left[\sin(k(x+y)) - \sin(k(x-y)) \right] \mathbf{e}_x + \nabla \chi(x, y). \quad (32)$$

The gradient $\nabla \chi(x, y)$ and the constant ϕ_0 may be chosen arbitrarily.

Figure 2 shows the total active intensity and its components for the presented case when the amplitude ratio is $A = 2B$. The results are displayed over a surface of dimensions 1.5λ by 1.5λ , where λ is the wavelength. The irrotational intensity in equation (29) and Figure 2(b) does not contain a coupling term between the waves. It depends only on the intensity of the wave propagating in the x -direction. The rotational intensity in equation (31) and Figure 2(c) is due to interference and its spatial average is zero. Finally, the irrotational component $\mathbf{I}_\phi(x, y)$ is equal to the spatial average of the active intensity field $\mathbf{I}(x, y)$ (Figure 2a) on any square with side length λ .

To summarize, the results illustrate that the irrotational component relates to the power flow and the rotational component to interference effects.

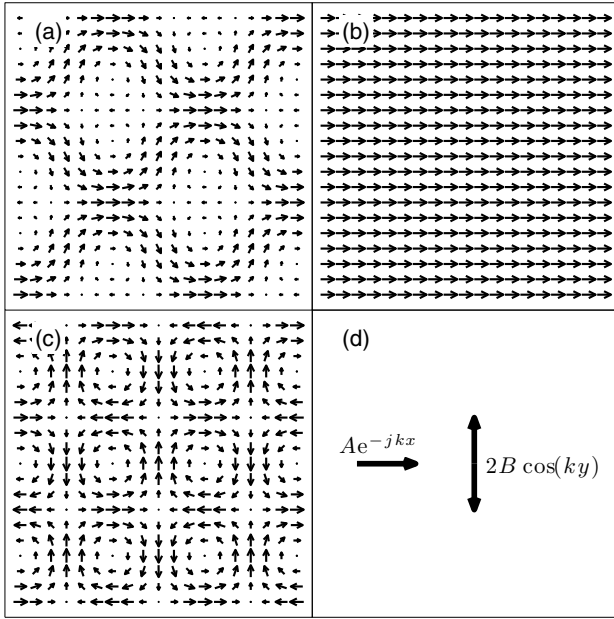


Figure 2. Interference between two plane perpendicular waves, one traveling wave along x and one standing wave along y : (a) active intensity, (b) irrotational intensity, (c) rotational intensity, and (d) directions of the waves. Figure adapted from Pascal [18].

3.2. Uncorrelated monopoles

The next intensity field under study is the one resulting from a distribution of uncorrelated monopole sources. Uncorrelated monopole sources are commonly assumed in high-frequency approaches. A monopole source radiating in free field leads to a spherical wave field. The intensity field from several uncorrelated monopoles is the sum of the intensity fields from the individual monopoles without any coupling terms,

$$\mathbf{I}(\mathbf{r}) = \sum_i \frac{w_i}{4\pi R_i^2} \mathbf{e}_{R_i} \quad (33)$$

where R_i is the distance from the monopole to the considered point, $w_i = 2\pi p_i^2 / \rho c$ is the power of the monopole, p_i is its amplitude, ρ and c are the density and speed of sound of the medium, and \mathbf{e}_{R_i} is the unit vector in radial direction from the monopole i .

As for the case of only one monopole, the active intensity can be derived from a single scalar potential:

$$\phi(\mathbf{r}) = \sum_i \frac{w_i}{4\pi R_i} \quad (34)$$

The constant of integration (ϕ_0 in equation 9) is chosen as zero so that $\phi(\mathbf{r})$ tends towards zero at infinity.

Another approach to calculate the irrotational active intensity field is to solve the Poisson equation when the volume densities of the power sources are given:

$$\nabla \cdot \mathbf{I}(\mathbf{r}) = -\Delta\phi(\mathbf{r}) = \sum_i w_i \delta(\mathbf{r} - \mathbf{r}_i), \quad (35)$$

where $\delta(\mathbf{r} - \mathbf{r}_i)$ is the Dirac function. The solution of this equation gives directly the potential $\phi(\mathbf{r})$ (equation 34) and its gradient gives the irrotational intensity.

3.3. Monopole above a reflecting surface

Pascal and Li [20] treated the case of a monopole radiating at a distance h from a reflecting surface. The interference between the monopole source and the image monopole is taken into account to calculate the active intensity and its irrotational and rotational components. A particular case is presented here to illustrate the behavior of these two components of intensity at higher frequencies.

The scalar potential $\phi(\mathbf{r})$ is the solution to the Poisson equation according to

$$\nabla \cdot \mathbf{I}(\mathbf{r}) = -\Delta\phi(\mathbf{r}) = w_h \delta(\mathbf{r} - \mathbf{r}_0) + w_h \delta(\mathbf{r} - \mathbf{r}'_0), \quad (36)$$

where \mathbf{r}_0 is the position of the monopole, and \mathbf{r}'_0 the position of the imaged monopole. The parameter w_h expresses the power delivered by the monopole located at the distance h from a reflecting plane of infinite extension, and w_0 is the power of the same monopole when placed in free field,

$$w_h = w_0 \left(1 + \frac{\sin(2kh)}{2kh} \right). \quad (37)$$

When the product of the wave number k and the height h goes to zero, the power of the source goes to twice the power of the monopole in free field. On the other hand, when the product kh is large, the power of the source is close to that of the monopole in free field.

The solution of equation (36) gives the scalar potential according to

$$\phi(\mathbf{r}) = w_h \left(\frac{1}{4\pi R} + \frac{1}{4\pi R'} \right), \quad (38)$$

where $R = \|\mathbf{r} - \mathbf{r}_0\|$ and $R' = \|\mathbf{r} - \mathbf{r}'_0\|$ are the distances from the monopole source and its image source, respectively, to the point \mathbf{r} . The irrotational intensity is obtained by calculating the gradient of $\phi(\mathbf{r})$ according to

$$\mathbf{I}_\phi(\mathbf{r}) = w_h \left(\frac{1}{4\pi R^2} \mathbf{e}_R + \frac{1}{4\pi R'^2} \mathbf{e}_{R'} \right), \quad (39)$$

where

$$\mathbf{e}_R = \frac{\mathbf{r} - \mathbf{r}_0}{\|\mathbf{r} - \mathbf{r}_0\|}, \mathbf{e}_{R'} = \frac{\mathbf{r} - \mathbf{r}'_0}{\|\mathbf{r} - \mathbf{r}'_0\|}, \quad (40)$$

are the unit vectors in radial direction of the source and its image source, respectively. The rotational intensity is calculated by subtraction as

$$\mathbf{I}_C(\mathbf{r}) = \frac{w_0}{4\pi} \left[\frac{\cos(k(R - R'))}{RR'} (\mathbf{e}_R + \mathbf{e}_{R'}) + \frac{\sin(k(R - R'))}{RR'} \left(\frac{\mathbf{e}_R}{kR} - \frac{\mathbf{e}_{R'}}{kR'} \right) - \frac{\sin(2kh)}{2kh} \left(\frac{\mathbf{e}_R}{R^2} + \frac{\mathbf{e}_{R'}}{R'^2} \right) \right]. \quad (41)$$

Figure 3 shows the typical intensity fields at high frequencies generated by a monopole placed on the vertical z -axis

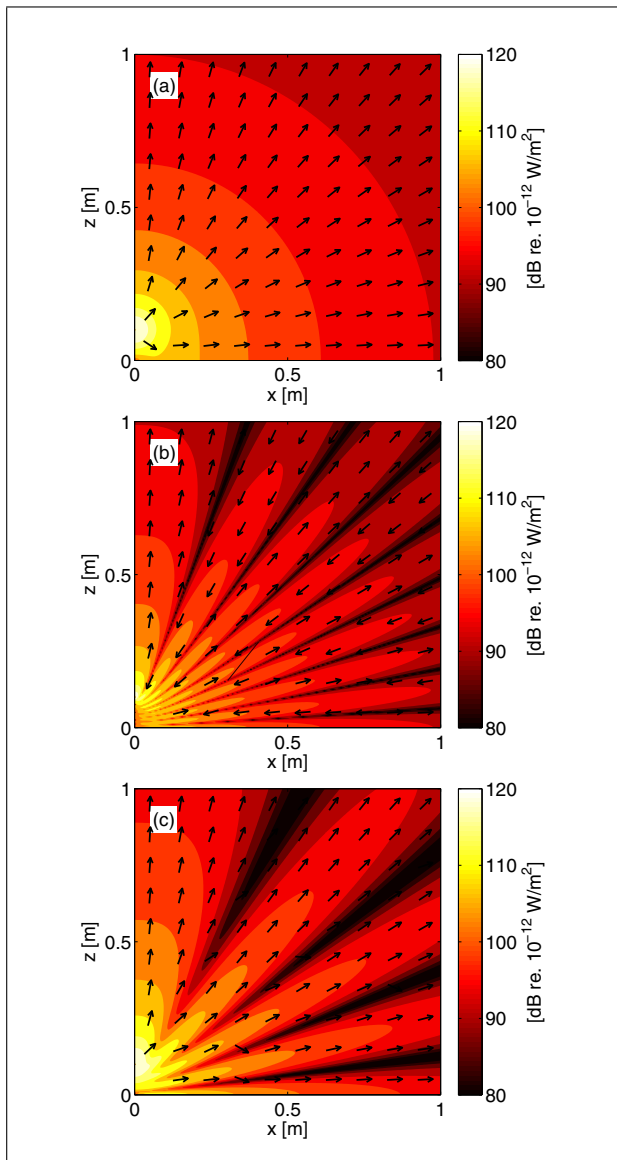


Figure 3. (a) Irrotational intensity, (b) rotational intensity, and (c) total intensity for $\lambda/h = 0.5$.

at the distance $h = 10$ cm from a reflecting plane. It also shows the decomposition by the Helmholtz theorem into the irrotational and rotational intensity. The case presented corresponds to a ratio of $1/2$ between wavelength λ and the distance h . The corresponding frequency is about 6800 Hz. The colors indicate the amplitude of the magnitude of irrotational, rotational, and total active intensity, according to a logarithmic scale (dB re. 10^{-12} W/m²). The arrows indicate the direction of the intensity.

The rotational intensity is locally on the order of the irrotational intensity and is alternately in the same or opposite direction. A very marked directivity pattern is created. The five lobes of directivity of the active intensity come from a strong rotational intensity directed in the same direction as the irrotational intensity, and the four shadow zones correspond to a strong rotational intensity which is opposite to the irrotational intensity.

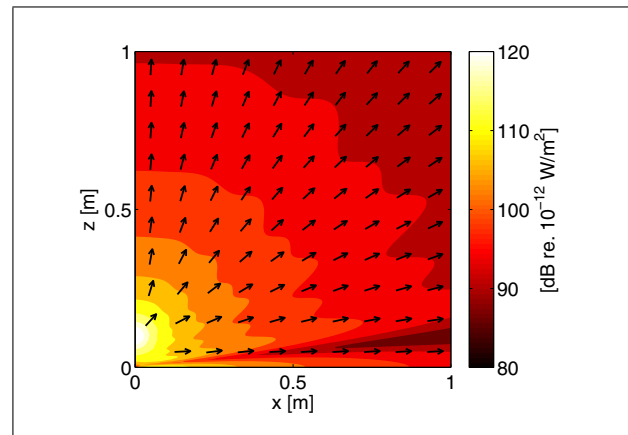


Figure 4. Total intensity for a broadband power source in the 8 kHz octave band.

For completeness, the behaviour at low and intermediate frequencies is here briefly described without figures. At low frequencies, the intensity is primarily irrotational. For instance, the rotational intensity is approximately 20 dB lower than the irrotational intensity when $\lambda = 50h$, $f = 68$ Hz and $h = 10$ cm. The power radiated by the monopole is 1.99 times larger than the power radiated by the same monopole in free field. At the intermediate frequencies, the rotational intensity is locally on the order of the irrotational intensity. The rotational intensity vector is alternately in the same or opposite direction as the irrotational intensity vector. A relatively marked directivity pattern is created.

3.4. Intensity in wider frequency bands

The results in Figures (2) and (3) show the fundamental properties of the components of the intensity field for a single frequency. Like all energy-based models, the intensity potential approach as a prediction tool is more applicable for wide frequency bands than for a single frequency. Figure 4 illustrates the total intensity in the 8 kHz octave band from a broadband source for the same geometry as in the previous example. The broadband source has a source strength w_0 that is constant over frequency. Hence, the power of the source is evenly distributed in the band.

The directivity pattern of the octave band total active intensity is very similar to the pattern given by the irrotational intensity. Figure 5 shows the total, irrotational, and rotational intensity at 1 m distance from the source as a function of angle to the normal of the reflecting ground. The total intensity at 1 m distance is roughly 94 dB re. 10^{-12} W/m². The rotational intensity is generally more than 10 dB lower than the irrotational or total intensity, and the rotational intensity has therefore little influence on the total intensity. The reason is that the number of lobes of the rotational intensity increases with frequency and their directions are changing with frequency. Thus, when integrating over a wide frequency band, the negative and positive lobes partly add up destructively and the importance of the irrotational intensity is in general reduced. The deviation between the total and the irrotational intensity is

generally less than 1 dB except close to grazing angle (see Figure 5). The total intensity is 8 dB lower in a lobe close to grazing angle and is 3 dB higher at the grazing angle.

In summary, the result shows that the irrotational intensity is a better representation of the total intensity when considering wide frequency bands compared to a single frequency.

3.5. Conclusions on intensity field decomposition

Whatever the frequency, the irrotational intensity field is not disturbed by the interference between waves. It has a smooth form whose attenuation is only due to the geometrical divergence. Only its amplitude varies with frequency because it is proportional to the in-situ power of the sources. On the boundary surfaces, the normal component of the irrotational intensity has the same boundary conditions as the total intensity. It is null on an acoustically hard surface and it goes to $1/2\pi R^2$ at large distances R from sources and objects. It fulfills the power balance for any arbitrarily chosen closed surface in terms of injected and dissipated power.

The rotational intensity field is directly related to the interference between waves, and therefore it varies radically with frequency. It is the cause of the directivity pattern of the total active intensity, being in the direction opposite to the irrotational intensity in certain regions, and being in the same direction in others. The influence of the rotational part is reduced when spatial and frequency averages of the active intensity are considered. Most important for the intensity potential approach is that the global balance of injected and dissipated power is independent of the rotational field.

4. Comparison to measured data

In this section, the intensity predicted by the intensity potential approach is evaluated for a three-dimensional case. Results of simulations are compared to results of intensity measurements. Special focus is put on directivity aspects. The studied case consists of a steel box that forms a partial enclosure.

4.1. Experimental setup

Figures 6 and 7 show the experimental setup. A steel box with a wall thickness of 3 mm is put on a platform. A compression chamber located below the top surface of the platform is connected to the box enclosure through a pipe. Its outlet is similar to a baffled circular piston of small dimensions (diameter 14 mm). The box has a small opening to the free field and forms a partial enclosure above the baffled piston. Results between 700 Hz and 3000 Hz are presented; the compression chamber emits little power at higher frequencies. In the range 700 Hz to 3000 Hz, the baffled piston has very little directivity because of its small dimensions. The power of the source has been determined indirectly by measurement of the intensity of the sound power radiating out of the opening of the box. The power

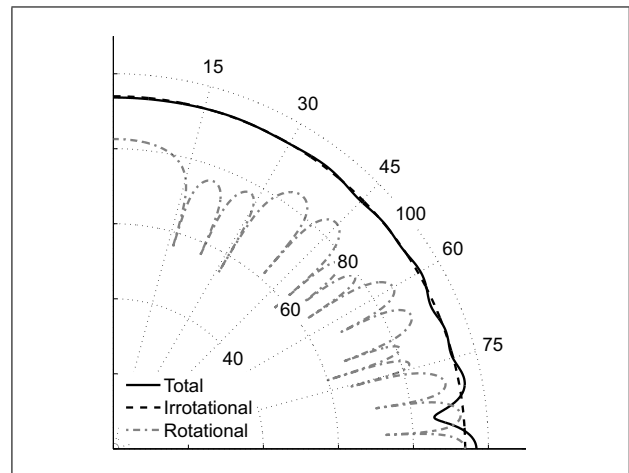


Figure 5. Magnitude of irrotational, rotational, and total intensity as a function of angle to the normal of the reflecting ground for a broadband power source in the 8 kHz octave band. [dB re. 10^{-12} W/m²].

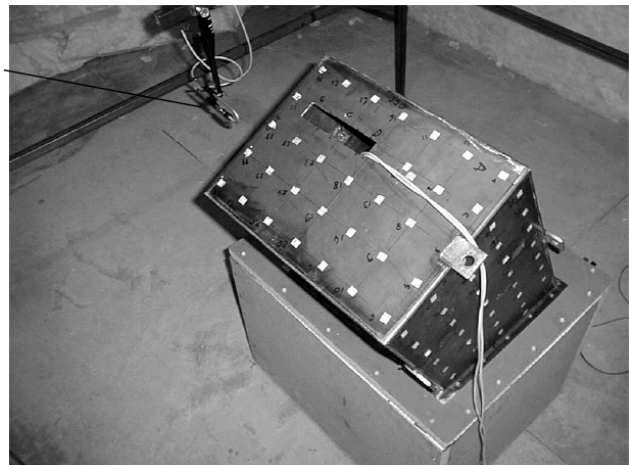


Figure 6. Enclosure with small opening without absorber.

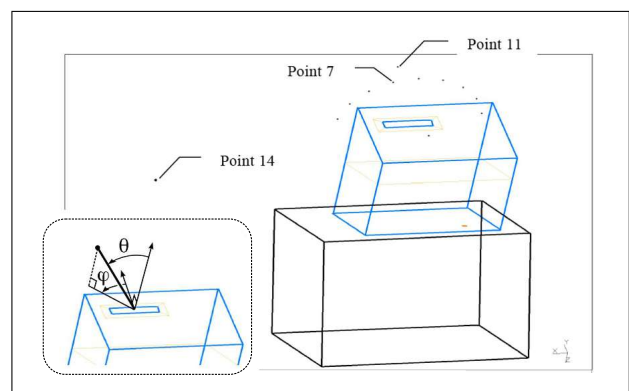


Figure 7. Position of the evaluation points and coordinate system.

transmission through the walls of the box is low, and the power of the source was assumed to be the power radiating through the opening in absence of absorption.

Intensity measurements are carried out at various points outside the steel box. The intensity probe visible in Figure 6 consists of two phase-matched Brüel & Kjær half-

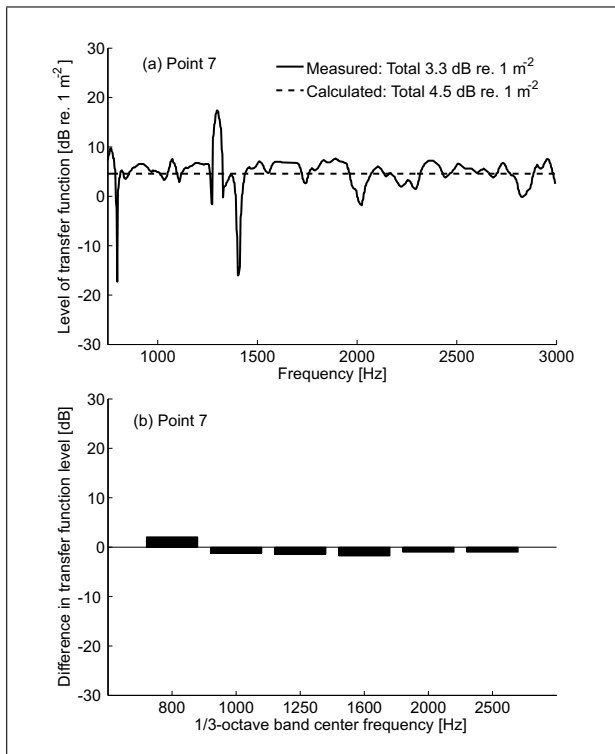


Figure 8. Comparison of the normalized energy transfer function $I_e(\mathbf{r}_j)/w_{\text{source}} = \mathbf{I}(\mathbf{r}_j)$ at point 7. (a) Levels in narrow band and (b) level difference between the measured results and the simulated results in 1/3-octave bands.

inch microphones. The amplitude of the active intensity in the considered direction is obtained by a finite difference approximation. A separation of 12 mm between the microphones allows covering the frequency range 700 Hz to 3000 Hz with an accuracy of 1 dB. The component of the measured intensity is divided by the source power to access the normalized energy transfer function $I_e(\mathbf{r}_j)/w_{\text{source}} = \mathbf{I}(\mathbf{r}_j) \cdot \mathbf{e}(\mathbf{r}_j)/w_{\text{source}}$, where $\mathbf{e}(\mathbf{r}_j)$ is the unit vector giving the direction of measured intensity at the considered point \mathbf{r}_j .

Table I gives the spherical coordinates of the measurement points labelled 7, 11 and 14. Figure 7 shows the coordinate system with origin in the centre of the aperture. The coordinate R is the radial distance to the origin. The coordinate θ is the inclination angle measured from a zenith direction that is perpendicular to the surface of the box in which the aperture is located. The coordinate φ is the azimuth angle in the plane of the same surface and the reference direction is shown in Figure 7.

4.2. Finite element calculation of the irrotational intensity

A standard heat transfer finite element solver was used to solve the intensity potential and resulting irrotational intensity for the presented case. The computation domain is the air volume inside and outside the box, limited by a half-sphere of 5 m radius. It is meshed with about 8900 linear tetrahedral elements. The mesh is refined in the vicinity of the source and geometric details. The radius R of

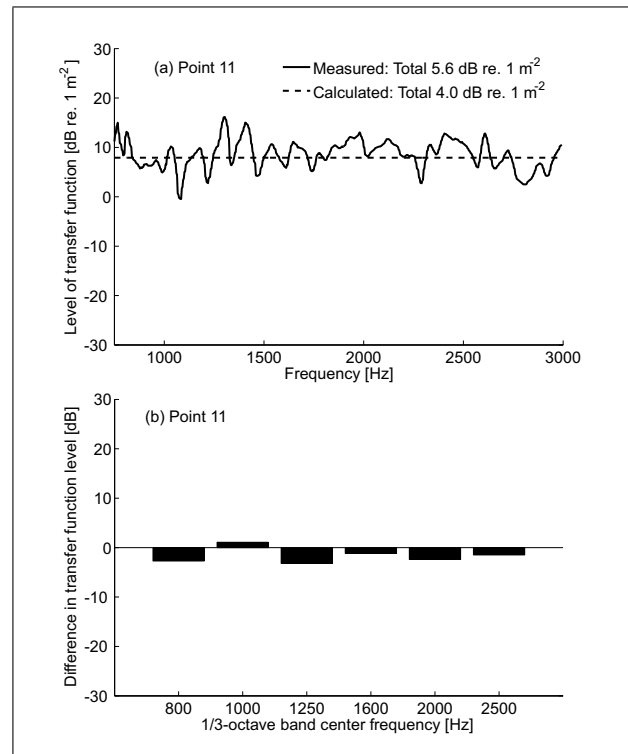


Figure 9. Comparison of the normalized energy transfer function $I_e(\mathbf{r}_j)/w_{\text{source}} = \mathbf{I}(\mathbf{r}_j)$ at point 11. (a) Levels in narrow band and (b) level difference between the measured results and the simulated results in 1/3-octave bands.

Table I. Coordinates of the evaluation points.

Point	R	θ	φ
7	0.21 m	20°	90°
11	0.21 m	60°	0°
14	0.60 m	120° (shadow zone)	90°

the half-sphere is slightly larger than five times the height of the box on its platform. The intensity potential approach calculation provides the vector field (3 components) of the irrotational intensity. The resulting vector in the measurement directions was used for the comparison. The calculation takes only a few minutes.

4.3. Comparison

The energy transfer functions (defined in section 4.1) from the intensity potential approach calculations and from experiments are compared. Figure 7 and Table I indicates the evaluation points labeled 7, 11, and 14 that are used in the comparison. The results in Figures 8–10 show that the energy transfer functions obtained by intensity potential approach in the absence of absorption are independent of frequency. The finite element calculation of the irrotational intensity estimates the overall level of active intensity (averaged over the entire frequency range) within ± 2 dB in points 7 and 11 (Figure 8–9) in the directly exposed region facing the opening. The difference between measured and calculated results is less than 3 dB in each 1/3-octave

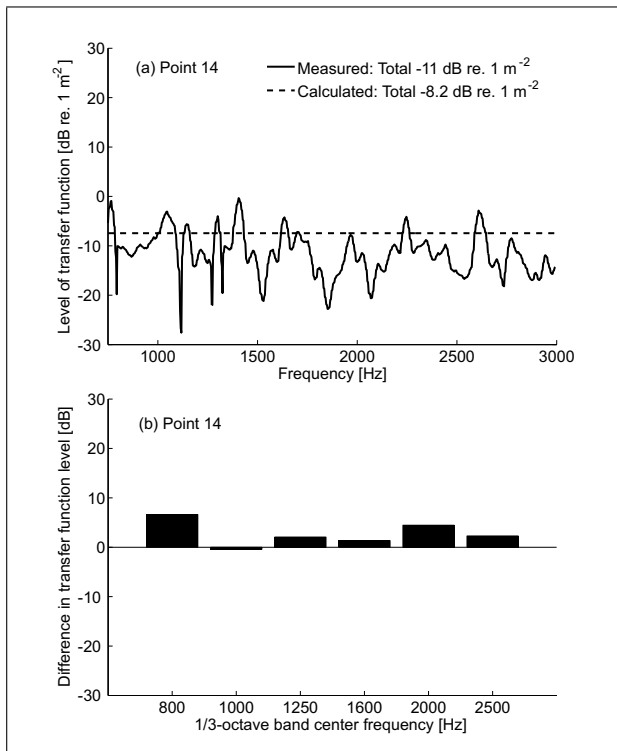


Figure 10. Comparison of the normalized energy transfer function $I_e(\mathbf{r}_j)/w_{\text{source}} = \mathbf{I}(\mathbf{r}_j)$ at point 14. (a) Levels in narrow band and (b) level difference between the measured results and the simulated results in 1/3-octave bands.

band, which is on the same order as the expected errors in the measured data. The comparison shows that the irrotational intensity component included in the calculations is linked to the power flow, which is in agreement to the theoretical derivation in section 2.3 and the demonstration examples in section 3. It is also clear that the method benefits from considering wider frequency bands as discussed in section 3.4.

The calculation overestimates the overall level of intensity by 2.8 dB in point 14 (Figure 10), which does not see the opening (diffracted field), and the difference reaches 6 dB in some 1/3-octave bands. Figure 11 shows the measured and calculated directivity along the width and length of the opening. All points used are above the box in the directly exposed region. The directivity is less pronounced in the results of the intensity potential approach calculation than in the results of the measured data (up to 2 dB difference). The rotational component is needed to describe the directivity in more detail as also demonstrated for a monopole above ground in section 3.3. To conclude, the directivity aspects are in general underestimated by the intensity potential approach since the rotational intensity component is not included in the calculations.

5. Conclusions

This paper has presented the intensity potential approach. The derivation of the governing equations has been accompanied by examples and comparison to measured data.

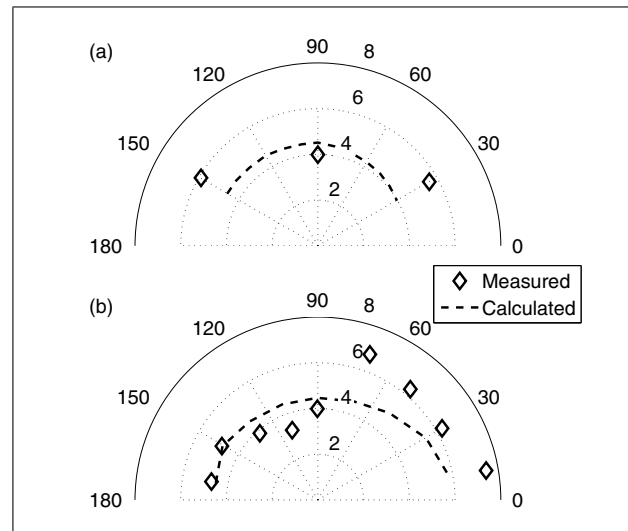


Figure 11. Directivity for the small opening along its width (a) and along its length (b). Average of the normalized energy transfer function in the range 700 Hz – 3000 Hz.

To summarize, the combination of the local energy balance (equation 6) in absence of volume dissipation and the decomposition of the active intensity (equation 7) into its irrotational and rotational components results in the Poisson equation for the acoustic intensity potential (equation 18). No additional assumptions or approximations apart from those behind the energy balance (equation 6) are introduced.

The intensity potential approach avoids the violation of geometrical divergence of acoustic energy in free field and the *assumption* of a Fourier type of law, which is not the case for the classical acoustic diffusion equation.

Equation (13) and the examples in section 3 clearly show that the irrotational intensity field is associated with the power flow. It is therefore reasonable to describe the propagation of acoustic energy by using only the irrotational component. Indeed, the theory predicts the global power correctly according to equation (20) (provided that the boundary conditions are correct).

For the rotational component, both the local (equation 15) and the global (equation 16) energy balance for any closed surface are always zero. The rotational field is associated with perturbations of the intensity field caused by interference between waves, which was demonstrated by the examples in section 3. However, the contribution from the rotational and reactive intensity is nevertheless important to estimate the power radiated from a source if only its volume velocity is given, or when the sound pressure in the near field is of interest. At larger distance from the sources and objects, the far-field assumption of plane wave impedance can be used for the approximate relation between the predicted intensity and the sound pressure.

Section 3.4 showed that the method is clearly more applicable when considering wide frequency bands. Introducing averaging/integration over more parameters, such as uncertainties in medium properties, source and receiver positions, and considering more complex geometry with

multiple sources, in general reduces the importance of the rotational component even more.

However, the method neglects directivity aspects and may therefore not always predict sound power radiated in certain directions or to certain regions with high accuracy. The comparison to measured data in section 4.3 revealed that the intensity in shielded zones is generally overpredicted by the approach.

The model and boundary condition of absorbing materials have not been discussed in this article. However, Thivant and Guyader [22, 23] have proposed to model absorbing materials by a spatially varying thermal convection factor based on an analogy to heat transfer problems and a diffuse field assumption. The development and evaluation of a relevant boundary condition for an absorber is a path of future research.

Acknowledgments

The work has mainly been performed within the research project “PREDIT ENCAPSULAGE”, and to a minor extent within the research project “Reduction of external noise for diesel propelled passenger cars”, sponsored by EMFO (Dnr AL 90B2004: 156660) and Vinnova/Green Car (Dnr 2005-00059). The funding is gratefully acknowledged.

Appendix

Radiation boundary condition corresponding to a perfectly absorbing surface

Let us consider the irrotational intensity field $\mathbf{I}_g(\mathbf{r}; \mathbf{r}_0)$ created by a point unit source located at \mathbf{r}_0 in an unbounded domain. This field derives from the scalar potential

$$g(\mathbf{r}; \mathbf{r}_0) = \frac{1}{4\pi\|\mathbf{r} - \mathbf{r}_0\|}, \quad (\text{A1})$$

which fulfills

$$\Delta g(\mathbf{r}; \mathbf{r}_0) = \delta(\mathbf{r} - \mathbf{r}_0). \quad (\text{A2})$$

The magnitude of the intensity vector is

$$\|\mathbf{I}_g(\mathbf{r}; \mathbf{r}_0)\| = -\frac{\partial g(\mathbf{r}; \mathbf{r}_0)}{\partial \hat{\mathbf{r}}(\mathbf{r})} = \frac{1}{4\pi\|\mathbf{r} - \mathbf{r}_0\|^2}, \quad (\text{A3})$$

and the vector points in the radial direction

$\hat{\mathbf{r}}(\mathbf{r}) = (\mathbf{r} - \mathbf{r}_0)/\|\mathbf{r} - \mathbf{r}_0\|$ from the origin of the source, and $\partial/\partial \hat{\mathbf{r}}(\mathbf{r})$ represents the directional derivative in the same direction.

Let us now solve the problem of a surface Γ_s of acoustic sources radiating in the volume Ω located between surface Γ_s and a large sphere of radius R centred on point \mathbf{r}_0 : $\Gamma_{r_0}(R)$. The scalar potential $\phi(\mathbf{r})$ must satisfy the two following equations:

$$\Delta \phi(\mathbf{r}) = 0 \quad \text{for } \mathbf{r} \in \Omega \quad (\text{A4})$$

and

$$\frac{\partial \phi(\mathbf{r})}{\partial \mathbf{n}(\mathbf{r})} = I_n^s(\mathbf{r}) \quad \text{for } \mathbf{r} \in \Gamma_s, \quad (\text{A5})$$

where $I_n^s(\mathbf{r})$ is a given distribution of injected intensity on the surface Γ_s . In addition, a boundary condition is required on the large sphere $\Gamma_{r_0}(R)$, which is the condition we want to identify in order to get a reflection-free boundary.

To identify the condition we start by calculating the integral

$$\iint_{\Omega} \Delta \phi(\mathbf{r}') g(\mathbf{r}', \mathbf{r}_0) d\Omega(\mathbf{r}') \quad (\text{A6})$$

as usually done in integral formulation. Because of equation (A4), the integral is equal to zero, and applying Green's identity we obtain

$$\begin{aligned} \phi(\mathbf{r}_0) = & \iint_{\Gamma_s} \frac{\partial g(\mathbf{r}', \mathbf{r}_0)}{\partial \mathbf{n}(\mathbf{r}')} \phi(\mathbf{r}') - \frac{\partial \phi(\mathbf{r}')}{\partial \mathbf{n}(\mathbf{r}')} g(\mathbf{r}', \mathbf{r}_0) d\Gamma(\mathbf{r}') \\ & + \iint_{\Gamma_{r_0}(R)} \left[\frac{\partial g(R, \theta, \varphi; \mathbf{r}_0)}{\partial R} \phi(R, \theta, \varphi) \right. \\ & \left. - \frac{\partial \phi(R, \theta, \varphi)}{\partial R} g(R, \theta, \varphi; \mathbf{r}_0) \right] R dR d\theta d\varphi, \end{aligned} \quad (\text{A7})$$

where (R, θ, φ) are the coordinates in a spherical coordinate system with origin at \mathbf{r}_0 . The first integral of the second member represents the contribution of the real sources; the second integral must vanish if no reflection occurs, as with radiation in an unbounded medium. In the second integral on the sphere $\Gamma_{r_0}(R)$, the normal derivative corresponds to the derivative towards the sphere radius, $\partial/\partial R$. Lastly, taking into account that the sphere is centered on point \mathbf{r}_0 , the following two expressions hold:

$$\frac{\partial g(R, \theta, \varphi; \mathbf{r}_0)}{\partial R} = -\frac{1}{4\pi R^2} \quad (\text{A8})$$

and

$$g(R, \theta, \varphi; \mathbf{r}_0) = \frac{1}{4\pi R}. \quad (\text{A9})$$

Incorporating the result in the integral and requiring it to be zero yields

$$\begin{aligned} \iint_{\Gamma_{r_0}(R)} \left[\frac{1}{R} \phi(R, \theta, \varphi) + \frac{\partial \phi(R, \theta, \varphi)}{\partial R} \right] \\ \cdot \frac{1}{4\pi R} R dR d\theta d\varphi = 0. \end{aligned} \quad (\text{A10})$$

It is clear from equation (A11) that the boundary condition allowing us to have $\phi(\mathbf{r})$ equal to the one in open space is

$$\frac{\partial \phi(R, \theta, \varphi)}{\partial R} = -\frac{1}{R} \phi(R, \theta, \varphi). \quad (\text{A11})$$

It must be noted here that this boundary condition leads to the expected result for a given point \mathbf{r}_0 , but to keep the

property when changing the calculation point necessitates also a change of the sphere centre, which is not realistic for finite element calculations. In practice, the sphere is fixed in space and the calculated results have insignificant errors if the points are far enough from the sphere surface. When the sphere radius tends to infinity, the calculation will be accurate for all finite locations and equation (A11) corresponds to the Sommerfeld condition at infinity.

References

- [1] C. Burroughs, R. Fisher, F. Kern: An introduction to statistical energy analysis. *Journal of the Acoustical Society of America* **101** (1997) 1779–1789.
- [2] R. Lyon, R. DeJong: Theory and application of statistical energy analysis. 2nd ed. Butterworth-Heinemann, Boston, 1995.
- [3] A. Le Bot, A. Bocquillet: Comparison of an intergal equation on the energy and the ray tracing technique in room acoustics. *Journal of the Acoustical Society of America* **108** (2000) 1732–1740.
- [4] J.-L. Guyader, T. Loyau: The frequency averaged quadratic pressure: a method for calculating the noise emitted by structures and for localizing the acoustic sources. *Acta Acustica united with Acustica* **86** (2000) 1021–27.
- [5] K.-K. Kim, J.-G. Ih: Prediction of sound level at high frequency bands by means of a simplified boundary element method. *Journal of the Acoustical Society of America* **112** (2002) 2645–2655.
- [6] J.-L. Guyader: Integral equation for frequency averaged quadratic pressure. *Acta Acustica united with Acustica* **90** (232-45) 2004.
- [7] L. Franzoni, D. Bliss, J. Rouse: An acoustic boundary element method based on energy and intensity variables for prediction of high frequency broadband sound fields. *Journal of the Acoustical Society of America* **110** (2001) 3071–80.
- [8] H. Kuttruff: Über den Nachhall in Medien mit unregelmäßig verteilten Streuzentren, insbesondere in Hallräumen mit aufgehängten Streuelementen (About the reverberation in media with irregularly distributed scattering centers, especially in reverberation chambers with hanging scattering elements). *Acustica* **18** (1967) 131–143.
- [9] E. Lindqvist: Sound-attenuation in large factory spaces. *Acustica* **50** (1982) 313–328.
- [10] J. Picaut, L. Simon, J.-D. Polack: A mathematical model of diffuse sound field based on a diffusion equation. *Acta Acustica* **83** (1997) 614–621.
- [11] J. Picaut: Modélisation des champs diffus par une équation de diffusion (Modelling of diffuse fields by an diffusion equation). PhD-thesis, l'Université du Maine, France, 1998.
- [12] T. Le Pollés, J. Picaut, S. Colle, M. Bérengier, C. Bardos: Sound-field modeling in architectural acoustics by a transport theory: Application to street canyons. *Phys. Rev. E* **72** 046609–1–046609–17 2005.
- [13] T. Schmitt: Diffraction and ground effects in simplified energy methods. Ninth International Congress on Sound and Vibration, Orlando, Florida, USA, 2002.
- [14] T. Schmitt: Modélisation des transferts acoustiques en moyennes et hautes fréquences par méthode énergétique: Application à l'encapsulation des compartiments moteurs (Modelling of acoustic transfer functions at medium and high frequencies by the energy method: Application to encapsulation of engine compartments). PhD-thesis, L'école centrale de Lyon, Lyon, France, 2004.
- [15] O. Bouthier, R. Bernhard: Simple models of energy flow in vibrating membranes. *Journal of Sound and Vibration* **182** (1995) 129–147.
- [16] R. Langley: On the vibrational conductivity approach to high frequency dynamics for two-dimensional structural components. *Journal of Sound and Vibration* **182** (1995) 637–657.
- [17] A. Le Bot: A vibroacoustic model for high frequency analysis. *Journal of Sound and Vibration* **211** (1998) 537–554.
- [18] J.-C. Pascal: Structure and patterns of acoustic intensity fields. Second International Congress on Acoustic Intensity, CET, Senlis, 1985, 97–104.
- [19] J.-C. Pascal, J.-F. Li: Irrotational acoustic intensity: A new method for location of sound sources. Sixth international congress on sound and vibration, Copenhagen, Denmark, 1999.
- [20] J.-C. Pascal, J.-F. Li: Irrotational acoustic intensity and boundary values. International Congress on Acoustics, Rome, Italy, 2001.
- [21] G. B. Arfken, H. J. Weber: Mathematical methods for physicists. International edition, 6th edition edition. Academic Press, San Diego, 2005.
- [22] M. Thivant, J.-L. Guyader: Introduction of sound absorbing materials in the intensity potential approach. Proceedings of 17th International Congress on Acoustics, Rome, Italy, 2001.
- [23] M. Thivant: Modélisation de la propagation acoustique par la méthode du potentiel d'intensité (Modelling of acoustic propagation by the intensity potential approach). PhD-thesis, l'INSA de Lyon, Lyon, France, 2003.